Decelerated Dark Flow Measured Using Steady-State Free Precession Magnetic Resonance Imaging for Specific Detection of Left Ventricular Myocardial Strain and Dyssynchrony in Dilated Cardiomyopathy

Kawakubo, Masateru
Department of Health Sciences, Faculty of Medical Sciences, Kyushu University

Nagao, Michinobu
Department of Diagnostic Imaging & Nuclear Medicine, Tokyo Women's Medical University

Nakao, Risako
Department of Cardiology, The Heart Institute of Japan, Tokyo Women's Medical University

Watanabe, Eri
Department of Cardiology, The Heart Institute of Japan, Tokyo Women's Medical University

他

出版情報：Cardiovascular Imaging Asia. 6 (1), pp.4-12, 2022-01-25. Asian Society of Cardiovascular Imaging
バージョン：

CVIA
ORIGINAL ARTICLE
pISSN 2508-707X / eISSN 2508-7088
https://doi.org/10.22468/cvia.2021.00339
Cardiovasc Imaging Asia 2022;6(1):4-12

Decelerated Dark Flow Measured Using Steady-State Free Precession Magnetic Resonance Imaging for Specific Detection of Left Ventricular Myocardial Strain and Dyssynchrony in Dilated Cardiomyopathy

Masateru Kawakubo[1], Michinobu Nagao[2], Risako Nakao[3], Eri Watanabe[3], Masami Yoneyama[4], Nobuhisa Hagiwara[3], Shuji Sakai[2]

[1]Department of Health Sciences, Faculty of Medical Sciences, Kyushu University, Fukuoka, Japan
[2]Department of Diagnostic Imaging & Nuclear Medicine, Tokyo Women's Medical University, Tokyo, Japan
[3]Department of Cardiology, The Heart Institute of Japan, Tokyo Women's Medical University, Tokyo, Japan
[4]Philips Electronics Japan, Ltd., Tokyo, Japan

Objective: In steady-state free precession (SSFP) cine imaging, signal loss can be observed as accelerated dark flow in patients with valvular disease and decelerated dark flow (DDF) in patients with severe left ventricular (LV) dysfunction. In our study, we measured DDF with optical flow calculations and investigated the relationship between DDF and myocardial strain or intraventricular dyssynchrony.

Materials and Methods: Fifty-seven consecutive patients with heart failure were retrospectively enrolled. In the short-axis orientation, the optical flow magnitude vector of the DDF was calculated over a cardiac cycle. The maximum value of the mean magnitude vector in the LV blood region was defined as the DDF index. The systolic circumferential strain (CS) of the LV free-wall, as well as the absolute difference in systolic timing of the LV free-wall and interventricular septum (LV dyssynchrony, LVD), was measured using the feature-tracking method. Spearman's correlation coefficients (ρ) were calculated between DDF and CS or LVD.

Results: Median and interquartile ranges (25th to 75th percentile) of measured DDF, CS, and LVD in 57 patients were 14.0 (10.3 to 20.4), -8.0% (-13.3 to -3.2), and 40 ms (21 to 99), respectively. There were statistically significant correlations between the values of DDF and CS as well as LVD (0.60 and 0.48; $p<0.01$ for both).

Conclusion: Measurement of DDF may provide a specific clinical picture of myocardial strain and intraventricular dyssynchrony. Furthermore, it is possible to cost-effectively measure DDF without additional image acquisition during routine MR examination.

Keywords Cine magnetic resonance imaging; Dilated cardiomyopathy; Heart ventricle; Medical image processing.

Received: September 17, 2021
Revised: November 18, 2021
Accepted: November 19, 2021

Corresponding author
Michinobu Nagao, MD, PhD
Department of Diagnostic Imaging & Nuclear Medicine,
Tokyo Women's Medical University,
8-1 Kawada-cho, Shinjuku-ku,
Tokyo, Japan
Tel: 81-3-3353-8111
Fax: 81-3-3353-8111
E-mail: nagao.michinobu@twmu.ac.jp

INTRODUCTION

Clinically, dark flow artifacts are frequently observed as signal loss in steady-state free precession (SSFP) cine cardiac magnetic resonance (CMR) imaging [1]. Dark flow artifacts typically arise from high-velocity blood flow through off-resonant points in the magnetic field [2,3]. Cardiac output is not predictable between cycles, and the artifacts are often exacerbated by cardiovascular diseases associated with irregular cardiac circu-

lation. For example, in patients with mitral valve regurgitation, signal loss is related to accelerated blood flow [4]. The area of signal loss may not directly reflect the severity of valve stenosis; however, it is a useful parameter for assessing the shape of defective heart valves and inferring the clinical consequences. Blood flow in the left ventricular (LV) blood pool stagnates in patients with severe heart failure (e.g., dilated cardiomyopathy [DCM]), presenting a risk for thrombus formation [5]. In patients with severe LV dysfunction, under low-velocity or stagnant blood conditions, decelerated dark flow (DDF) can still be observed on SSFP cine imaging. Thus, DDF can also be detected in low-velocity blood flow or stagnation. The prediction of responses to cardiac resynchronization therapy in DCM patients is clinically relevant, and DDF analysis using CMR has recently been reported to have predictive potential [6]. Furthermore, postoperative imaging after atriopulmonary connection-type Fontan surgery revealed an association between the presence of right atrium dark flow and the subsequent development of complications like supraventricular arrhythmia, thrombus formation, and liver disease [7,8]. Compared with dark flow, feature-tracking magnetic resonance imaging (FT-MRI) with SSFP cine imaging can quantify myocardial motion and dyssynchrony of the systolic timing in the myocardium with post-image processing [9-11], which is advantageous for clinical examination. As a result, FT-MRI is widely used in various clinical situations [12-15]. Late gadolinium enhancement (LGE) has also demonstrated an association between myocardial dyssynchrony and the presence of myocardial scarring [16,17]; however, to the best of our knowledge, the association between DDF in SSFP cine CMR imaging and myocardial function has not been fully investigated in patients with DCM. In our study, we sought to apply a unique imaging analysis algorithm to measure the DDF of cine MRI; using the algorithm, we evaluated the relatability of the DDF index value to cardiac strain, intraventricular dyssynchrony, and the presence of LGE.

MATERIALS AND METHODS

Patient population

This retrospective observational study was approved by the Institutional Review Boards of Tokyo Women's Medical University (No. 180309) and Kyushu University and was conducted in accordance with the 1964 Declaration of Helsinki. Written informed consent was waived by the institutional review boards. All data included in the study, including CMR imaging data, were derived from clinical examinations of patients with declining cardiac function. The sample comprised a consecutive series of 57 DCM patients, retrospectively enrolled, who had undergone CMR examinations for the assessment of LV function between January 2010 and December 2016 (40 men, 17 women; age, 48±18 years). Additional LGE imaging was performed in 55 of the 57 patients because two patients presented with renal complications; none of the patients had valvular disease or regurgitation. In all cases, an experienced radiologist (>10 years) confirmed the absence of jets in the SSFP CMR images. Patients were divided into the following three groups according to the guidelines of the American College of Cardiology [18]: 1) those with an LV ejection fraction (LVEF) >50% (indicative of normal LV function; 3 men, 5 women; age, 42±18 years); 2) those with an LVEF of 30%−50% (moderate or mild LV dysfunction; 12 men, 5 women; age, 43±15 years); and 3) those with an LVEF <30% (severe LV dysfunction; 25 men, 7 women; age, 52±18 years).

CMR imaging

CMR imaging was performed according to a previously published protocol [19]. A 1.5 T clinical scanner (Gyroscan Intera; Philips Medical Systems, Best, the Netherlands) with a four-element phased-array coil was used in the supine position with expiratory breath-holding and retrospective electrocardiogram gating. All SSFP cine images were acquired in the short-axis (SA), horizontal long-axis (HLA), and vertical long-axis (VLA) orientations. Parameters of cine imaging (20 frames/cardiac cycle) were as follows: repetition time, 2.8 ms; echo time, 1.4 ms; flip angle, 45°; slice thickness, 8 mm; slice gap, 0 mm; field of view, 380×380 mm^2; acquisition matrix, 176×193; reconstruction matrix, 352×352; parallel imaging acceleration factor (SENSE), 2.0. LGE imaging data were obtained 10 min after a 0.2 mmol/kg gadolinium injection (Magnevist; Bayer Healthcare, Osaka, Japan) with the following parameters: repetition time, 3.9 ms; echo time, 1.2 ms; flip angle, 15°; slice thickness, 4 mm; slice gap, 0 mm; spatial resolution, 1.32×1.79 mm^2.

CMR volume analysis

LV end-diastolic volume and end-systolic volume, which are the sums of the largest and smallest ventricular volumes (mL), respectively, were quantified from the SA image stack using manual planimetry of the endocardial borders and commercially available software (Vitrea; Canon Medical Systems Co., Tochigi, Japan). Both volumes were indexed to the body surface area and used to calculate ejection fractions (%). Stroke volume index was calculated as the difference between end-diastolic and end-systolic volume indices. Cardiac index was calculated as the product of stroke volume index and heart rate.

Strain measurement with cine CMR

LV regional strains were semi-automatically calculated using feature-tracking analysis as described previously [20]. All image processing algorithms for CMR imaging were implemented in MATLAB R2017b version 9.3 (Mathworks Inc., Natick, MA,

USA). At the end of diastole, regional endocardial borders were manually defined on the LV free-wall and interventricular septum in the SA and HLA images, and on the LV anterior and posterior walls in the VLA images (Fig. 1A). Endocardium points were then automatically tracked with manual correction over a cardiac cycle using a local template-matching technique based on normalized correlation coefficient values. In our study, the initial size of the template image and search area was 32×32 pixels. However, when the endocardium was not well tracked, the template size and search area were changed to ensure successful tracking. LV endocardial regions were automatically segmented as lines with spline interpolation and tracked over a cardiac cycle (Fig. 1B). Systolic regional strain and differences in systolic timing were calculated from the LV regional strain curves (Fig. 1C). Slice orientations SA and HLA were used to calculate the systolic circumferential (CS) and longitudinal strain (LS) of the free wall and interventricular septum, and the VLA slice orientation was used to cal-

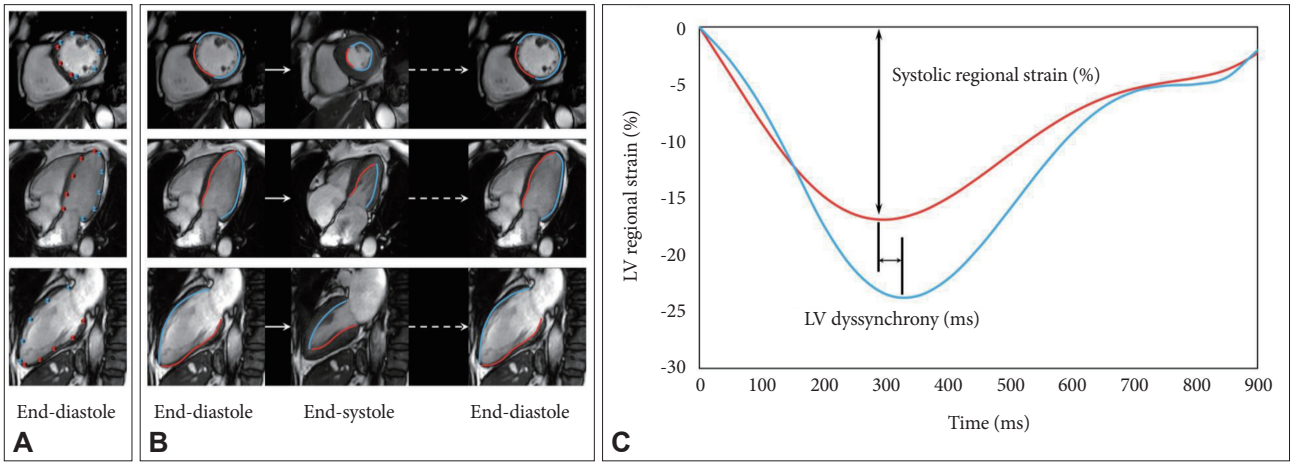

Fig. 1. Workflow of strain analysis with feature-tracking magnetic resonance imaging. A: Representative points of the endocardial region are manually determined at the end-diastolic phase (blue and red). B: The points are tracked over a cardiac cycle and interpolated as a spline curve. C: Regional time-strain curves are calculated by normalizing the lengths of the spline curves with the lengths at the end-diastole. Systolic myocardial strain and differences in systolic timing for each region are attainable using time-strain curves. LV, left ventricular.

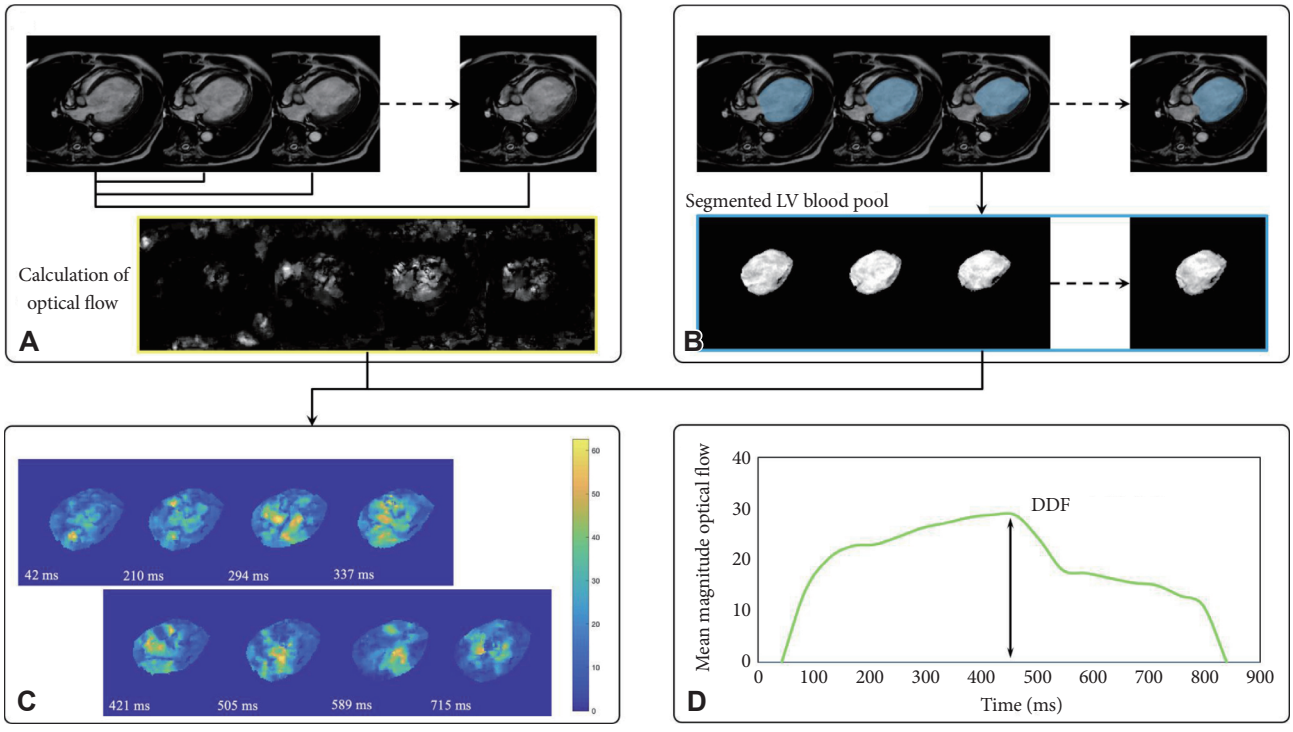

Fig. 2. Calculation of decelerated dark flow (DDF). A: Optical flows of steady-state free precession images at each cardiac phase with respect to the end-diastole. B: Left ventricular (LV) blood pooling regions. C: Movement magnitude vector in the LV blood pool. D: Mean magnitude vector in the LV blood pool.

Table 1. Baseline clinical characteristics of the study population

Parameter	Normal LV function	Moderate or mild LV dysfunction	Severe LV dysfunction	Kruskal-Wallis (p-value)	Dunn's post-hoc analysis (p-value)		
	LVEF >50%	30≤ LVEF ≤50%	LVEF <30%		Normal LV function vs. moderate or mild LV dysfunction	Normal LV function vs. severe LV dysfunction	Moderate or mild LV dysfunction vs. severe LV dysfunction
Number of patients	8	17	32				
Age (yr)	42 (26 to 56)	45 (28 to 57)	58 (43 to 65)	0.110	>0.999	0.480	0.200
Male/female	3/5	12/5	25/7				
BSA (m^2)	1.58 (1.41 to 1.88)	1.69 (1.63 to 1.83)	1.70 (1.55 to 1.80)	0.760	>0.999	>0.999	>0.999
BNP (pg/mL)	58 (24 to 125)	46 (6 to 154)	210 (112 to 614)	0.005*	>0.999	0.140	0.009*
NYHA classification							
I	8						
II		12					
III		5	7				
IV			25				
LGE	4/8	5/16	24/31				
HR (beats/min)	62 (57 to 67)	67 (62 to 76)	70 (61 to 88)	0.220	0.960	0.280	>0.999
LV function							
EDVi (mL/m^2)	65 (57 to 82)	80 (72 to 85)	151 (110 to 172)	<0.001*	>0.999	<0.001*	<0.001*
ESVi (mL/m^2)	30 (25 to 40)	45 (40 to 56)	122 (87 to 145)	<0.001*	0.860	<0.001*	<0.001*
EF (%)	52 (51 to 55)	41 (39 to 45)	17 (11 to 21)	<0.001*	0.240	<0.001*	<0.001*
SVi (mL/m^2)	37 (29 to 42)	32 (27 to 35)	23 (18 to 28)	0.001*	>0.999	0.002*	0.003*
CI ($L/min/m^2$)	2.3 (1.8 to 2.5)	2.2 (1.8 to 2.7)	1.6 (1.2 to 2.0)	0.002*	>0.999	0.020*	0.010*

Unless otherwise indicated, data are presented as medians [interquartile ranges (25th–75th percentile)]. *statistically significant p<0.05. LV, left ventricular; LVEF, left ventricular ejection fraction; BSA, body surface area; BNP, brain natriuretic peptide; NYHA, New York heart association; LGE, late gadolinium enhancement; HR, heart rate; EDVi, end-diastolic volume index; ESVi, end-systolic volume index; EF, ejection fraction; SVi, stroke volume index; CI, cardiac index

Table 2. Comparison of DDF and strains in the LV

	Normal LV function	Moderate or mild LV dysfunction	Severe LV dysfunction	Kruskal-Wallis (p-value)	Dunn's post-hoc analysis (p-value)		
	LVEF >50%	30≤ LVEF ≤50%	LVEF <30%		Normal LV function vs. moderate or mild LV dysfunction	Normal LV function vs. severe LV dysfunction	Moderate or mild LV dysfunction vs. severe LV dysfunction
Short-axis							
DDF	9.3 (7.9 to 9.7)	11.3 (7.9 to 13.0)	17.5 (14.0 to 26.1)	<0.001*	0.510	0.003*	0.005*
Free-wall CS (%)	-17.7 (-19.8 to -14.6)	-13.2 (-15.6 to -10.7)	-3.4 (-6.0 to -2.1)	<0.001*	>0.999	<0.001*	<0.001*
IVS CS (%)	-19.1 (-20.9 to -13.1)	-14.3 (-18.2 to -12.2)	-5.9 (-8.6 to -3.5)	<0.001*	>0.999	<0.001*	<0.001*
LVD (ms)	32 (8 to 59)	25 (10 to 37)	79 (38 to 154)	0.001*	>0.999	0.100	0.002*
Horizontal long-axis							
DDF	14.1 (12.6 to 20.3)	20.1 (16.7 to 27.3)	27.9 (20.1 to 39.0)	0.007*	0.500	0.01*	0.180
Free-wall LS (%)	-18.6 (-23.0 to -13.5)	-14.1 (-18.2 to -11.5)	-7.9 (-10.6 to -5.7)	<0.001*	0.860	<0.001*	<0.001*
IVS LS (%)	-14.2 (-16.8 to -11.9)	-10.3 (-12.8 to -8.4)	-5.8 (-8.7 to -3.1)	<0.001*	0.790	0.003*	0.001*
LVD (ms)	6 (0 to 47)	20 (13 to 36)	86 (51 to 149)	<0.001*	>0.999	0.004*	<0.001*
Vertical long-axis							
DDF	15.2 (13.4 to 17.2)	17.7 (15.7 to 21.1)	28.6 (20.0 to 42.2)	<0.001*	0.520	0.005*	0.008*
Anterior-wall LS (%)	-13.0 (-14.6 to -12.2)	-13.4 (-13.9 to -11.8)	-5.6 (-8.4 to -2.8)	<0.001*	>0.999	0.007*	<0.001*
Posterior-wall LS (%)	-11.8 (-17.9 to -8.8)	-11.1 (-14.7 to -10.2)	-8.9 (-11.5 to -5.4)	0.005*	>0.999	0.140	0.007*
LVD (ms)	26 (5 to 29)	31 (4 to 55)	64 (29 to 123)	0.007*	>0.999	0.030*	0.047*

Unless otherwise indicated, data are presented as medians [interquartile ranges (25th–75th percentile)]. *statistically significant p<0.05. LV, left ventricular; LVEF, left ventricular ejection fraction; DDF, decelerated dark flow; CS, circumferential strain; IVS, interventricular septum; LVD, left ventricular dyssynchrony

culate systolic LS of the anterior and posterior walls. LV dyssynchrony (LVD) was calculated as the absolute difference in systolic timing of any two regions in SA, HLA, and VLA, respectively.

DDF measurement with cine CMR

All image processing for DDF measurements was implemented in MATLAB R2017b version 9.3. Optical flows of SSFP images at each cardiac phase were computed with respect to the end-diastolic phase using the Lucas-Kanade algorithm and by solving the following optical flow constraint equation [21,22]:

$$I_x u + I_y v + I_t = 0,$$

where I_x, I_y, and I_t are the derivatives of spatiotemporal image brightness, and u and v are the horizontal and vertical image optical flows, respectively. The magnitude vector $|uv|$ was calculated using the following equation (Fig. 2A):

$$|uv| = \sqrt{u^2 + v^2}.$$

LV blood pooling regions, excluding papillary muscles, were isolated during a cardiac cycle by applying a threshold for signal intensity to the endocardium regions depicted by the feature-tracking algorithm used in the strain analysis (Fig. 2B). To avoid mixing endocardial contraction movement with the calculation area, the edge of the isolated area was reduced by erosion processing with a 3×3 pixel size. For standardized processing, the threshold was automatically determined using an adapted threshold method [23]. The magnitude vector of movement in the LV blood pool ($|uv|$) was obtained from the magnitude vector image by masking the LV blood pool region (Fig. 2C). Lastly, DDF was determined as the maximum point of the curve plotted using the mean magnitude vectors in the LV blood pool at each cardiac phase (Fig. 2D); DDF was calculated for all 57 patients in the SA, HLA, and VLA orientations.

Statistical analysis

The Shapiro-Wilk test for data normality was employed. Data with a non-normal distribution were summarized using descriptive statistics and are reported as medians and corresponding interquartile ranges (IQR). The Kruskal-Wallis non-parametric test with Dunn's post-hoc analysis was used for between-group comparisons. Spearman's correlation coefficients (ρ) for the DDF and CS values, LS values, and LVD values were calculated. Detectability of DDF in patients with CS and LS degradation >-10% [24] and with LVD longer than 50 ms [25] was evaluated by receiver operating characteristic (ROC) analysis. The ability of LGE to predict LVD longer than 50 ms was also evaluated by ROC analysis. All statistical analyses were conducted using GraphPad Prism (version 8.1.2 for Mac OS; GraphPad Software, La Jolla, CA, USA) with statistical significance set at $p<0.05$.

RESULTS

Baseline characteristics of the patients are displayed in Table 1. CMR examinations were successfully performed with sinus rhythm in all 57 patients. DDF values were significantly larger in patients with severe LV dysfunction than those with moderate or mild LV dysfunction as well as normal LV function. These findings were consistent across all slice orientations. Furthermore, CS, LS, and LVD were significantly decreased in the severe LV dysfunction group than in the other groups. Relationships between DDF and CS, LS, and LVD were statistically correlated. Between-group comparisons of DDF and CS, LS, and LVD are reported in Table 2, and Spearman's correlation coefficients for all 57 patients are reported in Table 3. Median and IQR of measured DDF, CS, and LVD in 57 patients were 14.0 (10.3 to 20.4), -8.0% (13.3 to -3.2), and 40 ms (21 to 99), respectively. DDF values were statistically correlated with strain and LVD in all slice orientations, and the ROC curves differentiating patients with strain degradation and prolonged LVD using DDF values are shown in Fig. 3. DDF parameters were measured in the SA orientation to determine free-wall CS, interventricular septum CS, and LVD (cut-off values of 13.0, 11.8, and 17.7; areas under the curves (AUCs [95% confidence interval]) of 0.78 [0.67−0.90], 0.79 [0.67−0.90], and 0.74 [0.60−0.87]; sensitivities of 44/57 [77%], 50/57 [88%], and 33/57 [58%]; and specificities of 45/57 [79%], 38/57 [67%], and 50/57 [88%], respectively). In the HLA orientation, free-wall LS, interventricular septum LS, and LVD were measured (cut-off values of 25.5,

Table 3. Spearman's correlation coefficient (ρ) and 95% CI between DDF and the value of strain and LVD

Strain parameter	DDF (95% CI)
Short-axis	
Free-wall CS (%)	0.60 (0.27 to 0.67)*
IVS CS (%)	0.55 (0.25 to 0.66)*
LVD (ms)	0.48 (0.36 to 0.72)*
Horizontal long-axis	
Free-wall LS (%)	0.48 (0.21 to 0.63)*
IVS LS (%)	0.39 (0.12 to 0.56)*
LVD (ms)	0.46 (0.10 to 0.56)*
Vertical long-axis	
Anterior-wall LS (%)	0.54 (0.34 to 0.71)*
Posterior-wall LS (%)	0.47 (0.21 to 0.63)*
LVD (ms)	0.35 (0.17 to 0.61)*

*p<0.01. DDF, decelerated dark flow; IVS, interventricular septum; CS, circumferential strain; LVD, left ventricular dyssynchrony; LS, longitudinal strain; CI, confidence interval

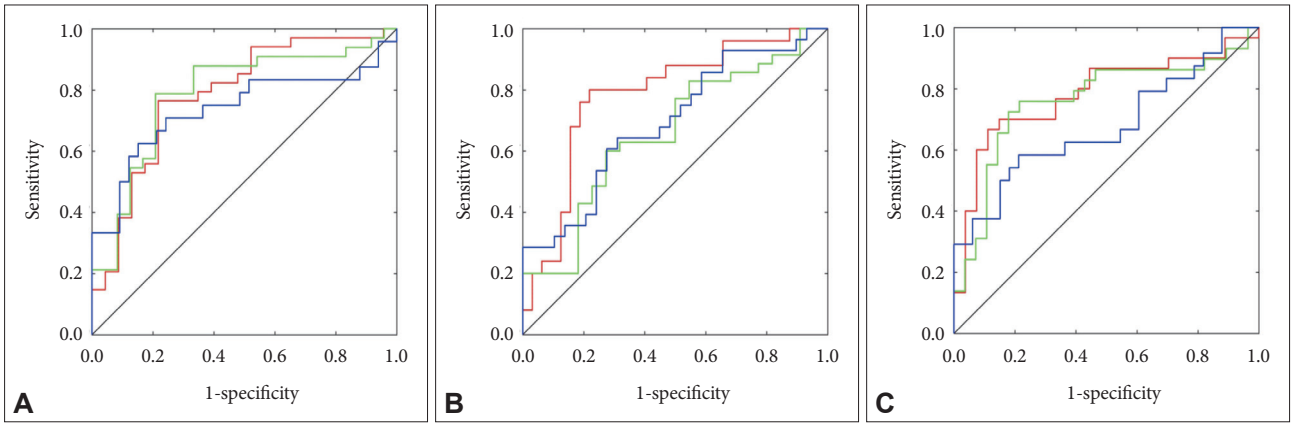

Fig. 3. Receiver operator characteristics curves for decelerated dark flow in short-, horizontal long-, and vertical long-axis orientations. A: Short-axis. B: Horizontal long-axis. C: Vertical long-axis. Red: detectability of strain <-10% for the free- or anterior wall; Green: detectability of strain <-10% for the interventricular septum or posterior wall; Blue: detectability of intraventricular dyssynchrony longer than 50 ms.

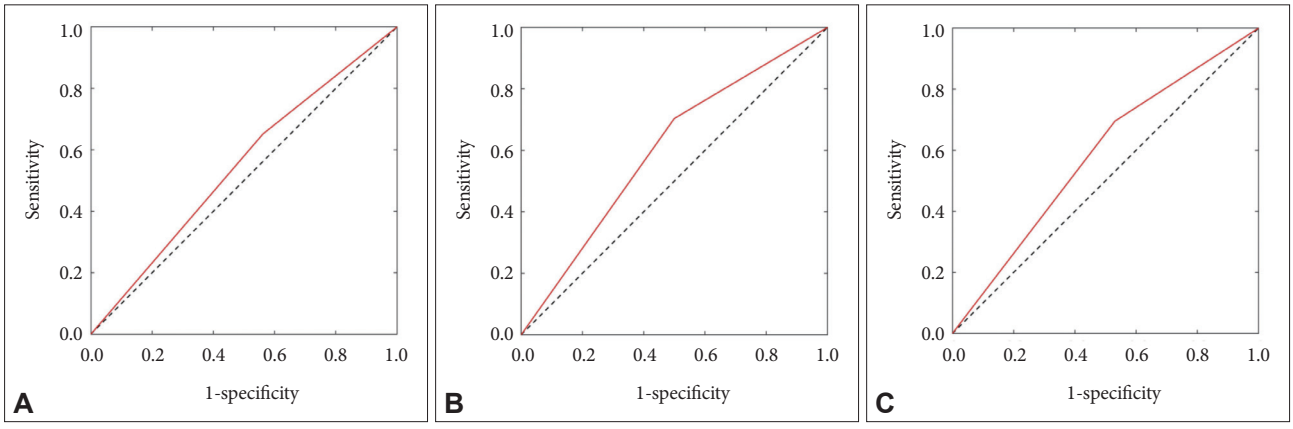

Fig. 4. Receiver operator characteristics curves for the presence of late gadolinium enhancement in short-, horizontal long-, and vertical long-axis orientations. A: Short-axis. B: Horizontal long-axis. C: Vertical long-axis.

19.1, and 25.2; AUCs of 0.78 [0.66–0.91], 0.66 [0.52–0.80], and 0.69 [0.56–0.83]; sensitivities of 43/57 [76%], 47/57 [83%], and 37/57 [64%]; and specificities of 46/57 [81%], 26/57 [45%], and 39/57 [69%], respectively). In the VLA orientation, anterior-wall LS, posterior-wall LS, and LVD were measured (cut-off values of 23.1, 21.1, and 43.9; AUCs of 0.78 [0.66–0.90], 0.76 [0.64–0.89], and 0.68 [0.53–0.82]; sensitivities of 38/57 [67%], 41/57 [72%], and 17/57 [30%]; and specificities of 51/57 [90%], 47/57 [83%], and 57/57 [100%], respectively). In the presence of LGE, LVD was predicted in the SA, HLA, and VLA orientations with an AUC of 0.54 [0.39–0.70], 0.60 [0.45–0.75], and 0.58 [0.43–0.74]; a sensitivity of 37/55 [67%], 40/55 [73%], and 40/55 [73%]; and a specificity of 32/55 [58%], 29/55 [53%], and 30/55 [55%], respectively (Fig. 4).

DISCUSSION

Data from the current study indicate a connection between DDF and LV myocardial dysfunction, supporting the potential use of DDF as an imaging tool (Table 2). Dark flow artifacts appear periodically during imaging with off-center resonance [3] and the intra-voxel phase dispersion effect is dependent on the echo time [2]. The presence of DDF is altered by magnetic field inhomogeneity conditions including magnetic field strength, patient body size, scan bore, metallic objects, and lung air. Signal loss caused by accelerated dark flow has been used by some researchers to assess the type and shape of heart valve defects [2]; however, any interpretation should be made with caution because no direct link between the area of signal loss and the severity of valve stenosis has been proven and the inter-scan reproducibility of signal loss cannot be guaranteed. Following the same line of reasoning for accelerated dark flow, clinical application of DDF measurements is tenuous. Moreover, DDF measurements are affected by the pixel size of SSFP MRI because the magnitude vector calculation is based on the pixelwise calculation with an optical flow algorithm. For clinical use of DDF analysis, further investigation of optimal pixel sizes and the effect of pixel size on DDF values are required. However, accord-

ing to ROC analyses, DDF measurements are capable of detecting degradation in myocardial strain and synchronized LV contraction with moderate performance. Based on our analyses, DDF performed better at detecting patients with myocardial dyssynchronization than LGE. Cases of heart transplantation for severe heart failure (e.g., DCM) are becoming more frequent. Heart motion after transplantation is considered unique because the shape and myocardium differ from the original heart, which may result in myocardial dyssynchrony. DDF measurement using the method described here has the potential to function as a clinical index for predicting the presence of dyssynchrony without use of a contrast medium in post-transplantation patients. However, further clinical evaluation and verification of the DDF measurement method proposed here are warranted.

We used FT-MRI to assess CS, LS, and LVD, as this is an established practice [12-15]. An advantage of FT-MRI, and where it differs from tagging MRI [26], is the possibility of post-imaging processing without acquisition of additional images other than those acquired during routine CMR examination. Processing techniques applied include displacement encoding with stimulated echoes (DENSE) imaging [27] and strain encoding (SENC) imaging [28]; both methods have proven reproducibility [29,30]. Similarly, DDF measurement may be useful for detecting myocardial dysfunction without additional image requirements. Furthermore, optical flow provides information about the magnitude and direction of motion in SSFP imaging. We propose that the analytic technique described has the potential to quantitatively evaluate vortex flow in the ventricular blood pool (see the Supplementary Video 1 in the online-only Data Supplement). A representative MR imaging technique to quantify blood flow velocity is the phase contrast technique. MR-derived blood flow velocity has recently been shown to be associated with energy loss of circulation in patients with pulmonary hypertension [31,32]. Our proposed DDF measurement method may in the future allow elucidation of the energy loss of the circulation caused by the combined effects of intraventricular blood stagnation and degraded ventricular wall motion. In other words, the dark flow shown here is mainly caused by slow flow, not by fast flow.

Our study has several limitations. Firstly, after assignment of patients to three groups, sample sizes were greatly reduced. Although we provided preliminary evidence of the clinical utility of DDF measurement with SSFP cine CMR imaging, there is scope for further verification in larger cohorts and using a prospective approach. Another limitation is the challenge of differentiating between DDF and accelerated dark flow. However, no patients in this study suffered from valvular disease and there was no jet present in any of the SSFP CMR images, so this challenge could not be directly addressed. Other functional parameters, excluding the cardiac index, were found to differ significantly between groups, possibly because of increased ventricular volume.

In conclusion, measurement of DDF with SSFP cine CMR imaging provides a clinical picture of LV myocardial dysfunction. Upon further confirmation, this approach is likely to constitute an improved and cost-effective tool for the clinical examination of patients with severe LV myocardial dysfunction.

Supplementary Video Legends

Video 1. Videos of steady-state free precession imaging (left) and a vector plot on the left ventricle blood pool (right) in patients with severe heart failure related to dilated cardiomyopathy. Calculated optical flow provides information about the magnitude and direction of motion. Our proposed analytic technique has the potential to quantitate vortex flow in the ventricular blood pool.

Supplementary Materials

The online-only Data Supplement is available with this article at https://doi.org/10.22468/cvia.2021.00339.

Conflicts of Interest

All authors claim no conflicts of interest concerning the study outcome. M.Y is an employee of Philips Electronics, Japan, but this is of no consequence to the study.

Acknowledgments

This work was awarded an ISMRM Travel Award by the Japanese Society for Magnetic Resonance in Medicine (JSMRM) in 2017. Portions of this study were reported at the 47th Annual Meeting of the JSMRM in 2019 and the 2018 Joint Annual Meeting ISMRM-ESMRMB. We thank Editage (www.editage.com) for the English-language editing of this article.

ORCID iDs

Masateru Kawakubo https://orcid.org/0000-0003-1867-1745
Michinobu Nagao https://orcid.org/0000-0001-6049-8857

Author Contributions

Conceptualization: Masateru Kawakubo, Michinobu Nagao. Data curation: Masami Yoneyama. Formal analysis: Masami Yoneyama, Masateru Kawakubo. Funding acquisition: Michinobu Nagao, Masateru Kawakubo. Investigation: Michinobu Nagao, Masateru Kawakubo. Methodology: Michinobu Nagao, Masateru Kawakubo. Project administration: Risako Nakao, Eri Watanabe. Resources: Risako Nakao, Eri Watanabe. Software: Masami Yoneyama, Risako Nakao. Supervision: Shuji Sakai, Nobuhisa Hagiwara. Validation: Michinobu Nagao, Masateru Kawakubo. Visualization: Michinobu Nagao, Masateru Kawakubo. Writing—original draft: Masateru Kawakubo. Writing—review & editing: Nobuhisa Hagiwara, Shuji Sakai.

REFERENCES

1. Li W, Storey P, Chen Q, Li BS, Prasad PV, Edelman RR. Dark flow artifacts with steady-state free precession cine MR technique: causes and implications for cardiac MR imaging. Radiology 2004;230:569-575.
2. Ferreira PF, Gatehouse PD, Mohiaddin RH, Firmin DN. Cardiovascular magnetic resonance artefacts. J Cardiovasc Magn Reson 2013;15:41.
3. Storey P, Li W, Chen Q, Edelman RR. Flow artifacts in steady-state free precession cine imaging. Magn Reson Med 2004;51:115-122.
4. Uretsky S, Argulian E, Narula J, Wolff SD. Use of cardiac magnetic resonance imaging in assessing mitral regurgitation: current evidence. J Am Coll Cardiol 2018;71:547-563.
5. Baccani B, Domenichini F, Pedrizzetti G, Tonti G. Fluid dynamics of the left ventricular filling in dilated cardiomyopathy. J Biomech 2002;35:665-

671.
6. Nakao R, Nagao M, Fukushima K, Sakai A, Watanabe E, Kawakubo M, et al. Prediction of cardiac resynchronization therapy response in dilated cardiomyopathy using vortex flow mapping on cine magnetic resonance imaging. Circ Rep 2019;1:333-341.
7. Shiina Y, Inai K, Takahashi T, Shimomiya Y, Ishizaki U, Fukushima K, et al. Vortex flow in the right atrium surrogates supraventricular arrhythmia and thrombus after atriopulmonary connection-type Fontan operation: vortex flow analysis using conventional cine magnetic resonance imaging. Pediatr Cardiol 2018;39:375-383.
8. Ishizaki U, Nagao M, Shiina Y, Fukushima K, Takahashi T, Shimomiya Y, et al. Prediction of Fontan-associated liver disease using a novel cine magnetic resonance imaging "vortex flow map" in the right atrium. Circ J 2018; 82:2143-2151.
9. Pedrizzetti G, Claus P, Kilner PJ, Nagel E. Principles of cardiovascular magnetic resonance feature tracking and echocardiographic speckle tracking for informed clinical use. J Cardiovasc Magn Reson 2016;18:51.
10. Schuster A, Hor KN, Kowallick JT, Beerbaum P, Kutty S. Cardiovascular magnetic resonance myocardial feature tracking: concepts and clinical applications. Circ Cardiovasc Imaging 2016;9:e004077.
11. Hor KN, Baumann R, Pedrizzetti G, Tonti G, Gottliebson WM, Taylor M, et al. Magnetic resonance derived myocardial strain assessment using feature tracking. J Vis Exp 2011;48:2356.
12. Kawakubo M, Yamasaki Y, Kamitani T, Sagiyama K, Matsuura Y, Hino T, et al. Clinical usefulness of right ventricular 3D area strain in the assessment of treatment effects of balloon pulmonary angioplasty in chronic thromboembolic pulmonary hypertension: comparison with 2D feature-tracking MRI. Eur Radiol 2019;29:4583-4592.
13. Kawakubo M, Arai H, Nagao M, Yamasaki Y, Sanui K, Nishimura H, et al. Global left ventricular area strain using standard two-dimensional cine magnetic resonance imaging with inter-slice interpolation. Cardiovasc Imaging Asia 2018;2:187-193.
14. Heermann P, Fritsch H, Koopmann M, Sporns P, Paul M, Heindel W, et al. Biventricular myocardial strain analysis using cardiac magnetic resonance feature tracking (CMR-FT) in patients with distinct types of right ventricular diseases comparing arrhythmogenic right ventricular cardiomyopathy (ARVC), right ventricular outflow-tract tachycardia (RVOT-VT), and Brugada syndrome (BrS). Clin Res Cardiol 2019;108:1147-1162.
15. Nagao M, Yamasaki Y. Cardiac strain analysis using cine magnetic resonance imaging and computed tomography. Cardiovasc Imaging Asia 2018; 2:76-84.
16. Kawakubo M, Nagao M, Kumazawa S, Chishaki AS, Mukai Y, Nakamura Y, et al. Evaluation of cardiac dyssynchrony with longitudinal strain analysis in 4-chamber cine MR imaging. Eur J Radiol 2013;82:2212-2216.
17. White JA, Yee R, Yuan X, Krahn A, Skanes A, Parker M, et al. Delayed enhancement magnetic resonance imaging predicts response to cardiac resynchronization therapy in patients with intraventricular dyssynchrony. J Am Coll Cardiol 2006;48:1953-1960.
18. Yancy CW, Jessup M, Bozkurt B, Butler J, Casey DE, Colvin MM, et al. 2017 ACC/AHA/HFSA focused update of the 2013 ACCF/AHA guideline for the management of heart failure: a report of the American College of Cardiology/American Heart Association Task Force on Clinical Practice Guidelines and the Heart Failure Society of America. J Am Coll Cardiol 2017;70:776-803.
19. Kawakubo M, Nagao M, Ishizaki U, Shiina Y, Inai K, Yamasaki Y, et al. Feature-tracking MRI fractal analysis of right ventricular remodeling in adults with congenitally corrected transposition of the great arteries. Radiol Cardiothorac Imaging 2019;1:e190026.
20. Kawakubo M, Nagao M, Kumazawa S, Yamasaki Y, Chishaki AS, Nakamura Y, et al. Evaluation of ventricular dysfunction using semi-automatic longitudinal strain analysis of four-chamber cine MR imaging. Int J Cardiovasc Imaging 2016;32:283-289.
21. Lucas BD, Kanade T. An iterative image registration technique with an application to stereo vision. 7th International Joint Conference on Artificial Intelligence (IJCAI), 1981 Aug 24-28, Vancouver. Pittsburgh, Computer Science Department, Carnegie-Mellon University, 1981. p.674-679.
22. Barron JL, Fleet DJ, Beauchemin SS. Performance of optical flow techniques. Int J Comput Vis 1994;12:43-77.
23. Bradley D, Roth G. Adaptive thresholding using the integral image. J Graph Tools 2007;12:13-21.
24. Moreira HT, Nwabuo CC, Armstrong AC, Kishi S, Gjesdal O, Reis JP, et al. Reference ranges and regional patterns of left ventricular strain and strain rate using two-dimensional speckle-tracking echocardiography in a healthy middle-aged black and white population: the CARDIA study. J Am Soc Echocardiogr 2017;30:647-658.e2.
25. Richardson M, Freemantle N, Calvert MJ, Cleland JG, Tavazzi L; CARE-HF Study Steering Committee and Investigators. Predictors and treatment response with cardiac resynchronization therapy in patients with heart failure characterized by dyssynchrony: a pre-defined analysis from the CARE-HF trial. Eur Heart J 2007;28:1827-1834.
26. Nagao M, Hatakenaka M, Matsuo Y, Kamitani T, Higuchi K, Shikata F, et al. Subendocardial contractile impairment in chronic ischemic myocardium: assessment by strain analysis of 3T tagged CMR. J Cardiovasc Magn Reson 2012;14:14.
27. Aletras AH, Ding S, Balaban RS, Wen H. DENSE: displacement encoding with stimulated echoes in cardiac functional MRI. J Magn Reson 1999; 137:247-252.
28. Pruessmann KP, Weiger M, Scheidegger MB, Boesiger P. SENSE: sensitivity encoding for fast MRI. Magn Reson Med 1999;42:952-962.
29. Alfakih K, Plein S, Thiele H, Jones T, Ridgway JP, Sivananthan MU. Normal human left and right ventricular dimensions for MRI as assessed by turbo gradient echo and steady-state free precession imaging sequences. J Magn Reson Imaging 2003;17:323-329.
30. Schmidt B, Dick A, Treutlein M, Schiller P, Bunck AC, Maintz D, et al. Intra- and inter-observer reproducibility of global and regional magnetic resonance feature tracking derived strain parameters of the left and right ventricle. Eur J Radiol 2017;89:97-105.
31. Nagao M, Yamasaki Y, Abe K, Hosokawa K, Kawanami S, Kamitani T, et al. Energy efficiency and pulmonary artery flow after balloon pulmonary angioplasty for inoperable, chronic thromboembolic pulmonary hypertension: analysis by phase-contrast MRI. Eur J Radiol 2017;87:99-104.
32. Nabeta T, Itatani K, Miyaji K, Ako J. Vortex flow energy loss reflects therapeutic effect in dilated cardiomyopathy. Eur Heart J 2015;36:637.